5th International Conference on Biaxial/Multiaxial Fatigue and Fracture
Cracow'97, Poland

Kenji Hatanaka*, N. Motozawa*,
H. Ogawa**, N. Sasaki*** and S.Rokukawa***

A Study on Fatigue Crack Growth under Biaxial Loadings Using Cruciform Specimen

* Department of Mechanical Engineering, Yamaguchi University, Ube, 755 Japan
** Department of Mechanical Engineering, Ube Technical College, Ube, 755 Japan
*** Japan Ultra-high Temperature Materials Research Center Ltd, Ube, 755 Japan

Keywords: Biaxial Fatigue, Cruciform Specimen, Crack Extention, Stress Intensity Factor, Stress/Strain Analysis

ABSTRACT: The appropriate cruciform specimen for biaxial fatigue was newly designed using the elastic finite element method and fatigue crack extension tests were performed under cyclic loadings at several biaxial stress ratios. Crack opening load point measured by means of an unloading elastic compliance method showed that a negative biaxial stress ratio T<0 increases a crack opening load ratio. The plastic strain was calculated around the crack tip under several static biaxial loading conditions using the elastic-plastic finite element method. Then the localized plastic strain was found to be developed much more under the condition of T<0 than T>0 in both the amount and the domain size.

The crack growth rate da/dN plotted against the stress intensity factor range exhibited the biaxial stress ratio dependency; the da/dN vs. ΔK plots are situated on the higher growth rate side under test conditions of T<0 than T>0. Such a biaxial stress ratio dependency disappears in the relationship between the crack growth rate and the effective stress intensity factor range ΔK_{eff} The crack extension behaviors under biaxial cyclic loadings mentioned above is reasonably interpreted in terms of the localized plastic deformation around the crack tip.

1 Introduction

Analytical and experimental works have been extensively conducted on fatigue under multiaxial stress loadings, since machine components are generally in such a stress state in service.[1]-[11] Some multiaxial fatigue behaviors, however, remain still unknown. For instance, the opinion is divided on the effect of the stress perpendicular to crack extension on fatigue crack growth; crack extension is accelerated by the compressive perpendicular stress and reduced by the tensile perpendicular stress in some test data[4]-[7], while other test data show that crack growth is hardly influenced by the tensile perpendicular stress[8]-[11].

Biaxial stress-fatigue tests are performed at biaxial stress ratios ranged much more widely in cruciform specimen than in thin-walled cylindrical specimen under the

combined loadings of tension and torsion. Then the cruciform specimen was used under biaxial tension- compression loadings in the present study.

Optimum design of the cruciform specimen is required for the biaxial fatigue test[1)4)-6)]; the stress must be greater in the central thickness-reduced region than in any other regions including four corners in the specimen .The appropriate configuration of the cruciform specimen, however, has not been standardized yet.

Stress analysis was numerically conducted for the cruciform specimen using the elastic finite element method, and then optimum configuration and dimensions of the cruciform specimen were determined.

Fatigue crack extension tests were performed for the cruciform specimen machined from JIS S45C steel which contains about 0.45 weight percent carbon. Then the effect of the biaxial stress on fatigue crack growth rate was examined in terms of the fracture mechanics. At that time the special attention was given to the measurement of crack closure and the analysis of localized plastic strain around the crack tip under biaxial loadings.

2 Test System

The Instron-closed loop type-biaxial push-pull fatigue test system with the capacity of $\pm$100kN was employed for the experimental works, where four actuators are installed, and the cyclic stress amplitude and the mean stress in the X- and Y-directions, and the phase difference in time between the two directions can be independently controlled. As the result, we can set up the biaxial principal stress ratio $\lambda = \sigma_2/\sigma_1$ at arbitrary values ranged from -1 to 1.0. The appearance of specimen-mounting part of the test system is presented in Fig,1. This test system is installed in the Japan Ultra-High Temperature Materials Research Center Ltd.(JUTEM).

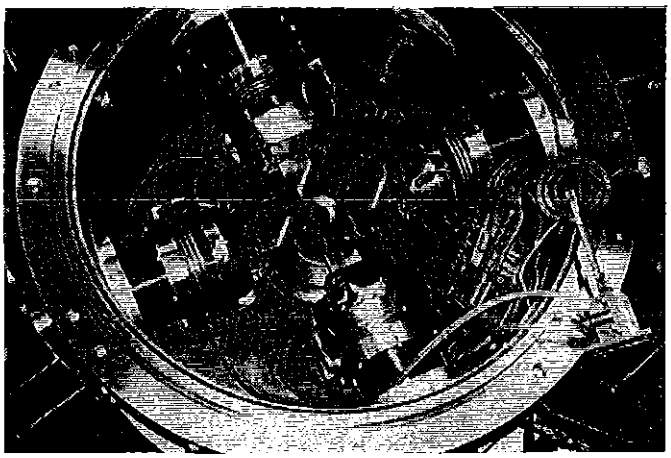

Fig. 1 Appearance of specimen-mounting part of the test system

3 Design of the Cruciform Specimen

An elastic stress analysis was carried out for the cruciform specimen using the general program for the finite element method-calculation MARC. K6, where an octant of the specimen was made an object of the calculation for its symmetrical configuration. Material's constants of Young's modulus, Poisson's ratio and yield stress are E= 206GPa, υ =0.3 and σ_y=270.7MPa ,respectively.

High stress region was built up in the central region of the specimen by reducing the thickness for crack not to originate at the four corners. Then stress analysis was carried out for the cruciform specimen with t=2 and 3mm in thickness at the center by means of the three dimensional elastic FEM. The eight node-isoparametric elements of which numbers are 604 and 1014 in the mesh element and the node were used. The mesh division is presented as an example in Fig.2. The stress analysis was performed for the specimen of t=2mm under the tensile equi-biaxial stress condition of $\sigma_{x0}=\sigma_{y0}=$ 78MPa, where $\sigma_{x0}=\sigma_{y0}$ are the stresses applied at the grip ends in the X-and Y-directions in Fig.2.

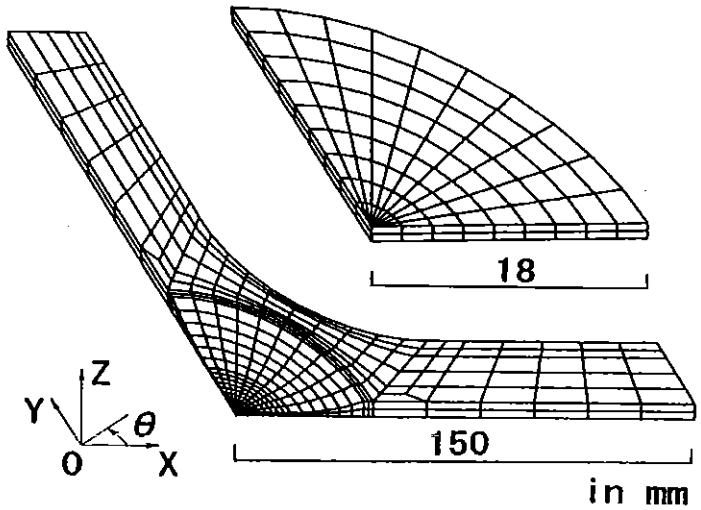

Fig. 2 Mesh division in FEM analysis. Angle inclined with respect to X-axis in X-Y plane is denoted by θ

Figures 3 show the distribution of the Mises type equivalent stress σ_{eq} calculated along the line inclined by θ=45° with respect to the X-axis in the X-Y plane in the specimen. Figure 3(a) shows the dependence of the equivalent stresses distribution on the curvature of round portion connecting the thickness-reduced region with the original thickness region R, which was calculated for the specimen preparing the thickness-reduced region within the circle of radius r_0=21.0mm.The uniform stress distribution is realized within r_0=21.0mm for the three values of R=20, 52 and 74mm in the figure. The stress, however, reaches the maximum at the beginning point in the thickness reduction for R=20mm. Meanwhile, such a phenomenon disappears for R=52 and 74

mm. Thus stress concentration occurring at this location attenuates with increase in the R-value. The increase in the R value ,however, makes the distance between the beginning point in the thickness reduction and the edge in the four corners reduce and probably fatigue crack initiate at the edge of the four corners. The curvature given in the thickness-reduced region was determined as R=74mm from such a consideration.

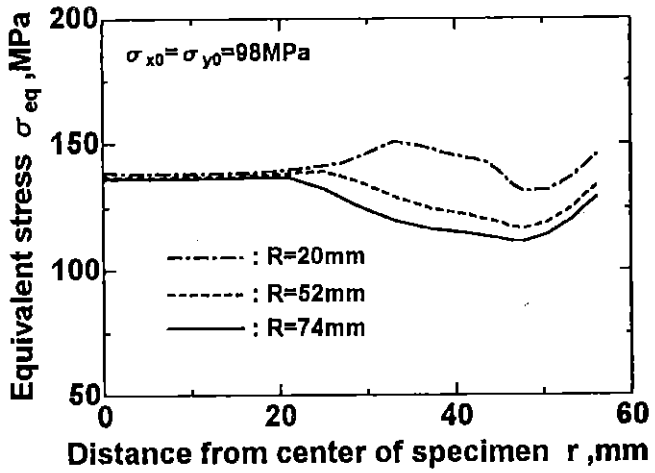

(a) Effect of curvature R at the arc-shaped thickness-reduced portion on the stress distribution in Type A specimen, where t=2mm and r_0=21mm are settled.

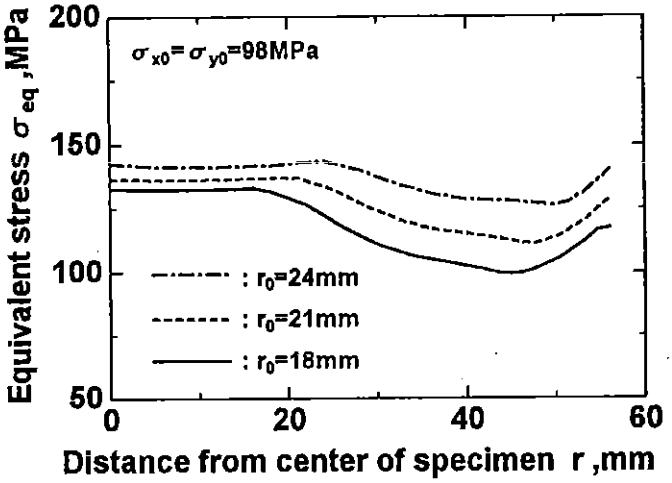

(b) Effect of radius r_0 of thickness-reduced region on the stress distribution, where t=2mm and R=74mm are settled

Fig. 3 Distribution of equivalent stress in the direction of θ=45° calculated in theTypeA cruciform specimen under equi-biaxial loadings of σ_{x0}= σ_{y0}=98MPa.

Figure 3(b) shows the effect of the radius of the thickness-reduced region r_0 on the equivalent stress distribution, which was calculated by setting t=2mm and R=74mm under the loading condition of $\sigma_{x0}=\sigma_{y0}$=98MPa. According to the figure, the stress varies with a gentle slope in the thickness-reduced region and reach the maximum at the beginning point of the thickness reduction for r_0=24mm. Such a stress variation disappears with decrease in r_0 from 24 to 18mm, and then nearly uniform stress distribution is attained in the thickness-reduced region for r_0=18mm. In addition the stress in the thickness-reduced region is higher than the one at the beginning point of the thickness-reduction for r_0=18mm.The radius of the thickness-reduced region r_0 was determined as 18mm from the above calculation.

Figures 4 (a), (b) and (c) show the stresses plotted against the distance from the center of the specimen in the X(θ=0°)-, θ=45° -and Y(θ=90°)-directions, respectively, which were calculated for the specimen with t=2mm, R=74mm and r_0=18mm under the equi-biaxial loading condition of $\sigma_{x0}=\sigma_{y0}$=78MPa.The figures show that the Mises type equivalent stress σ_{eq} remains constant within the radius of r=10mm in the three directions ,while the normal stresses in the X-and Y-directions, σ_x and σ_y vary outside the circle of r=10mm. The differences between the stresses at the center and r=10mm is less than 3.0 percent of the ones at the center, which holds under the equi-biaxial loading conditions other than $\sigma_{x0}=\sigma_{y0}$=78MPa. It was decided from the above calculations that the stress raising and the uniformity in the raised stress are realized within the circle of radius less than 10mm in the cruciform specimen. The

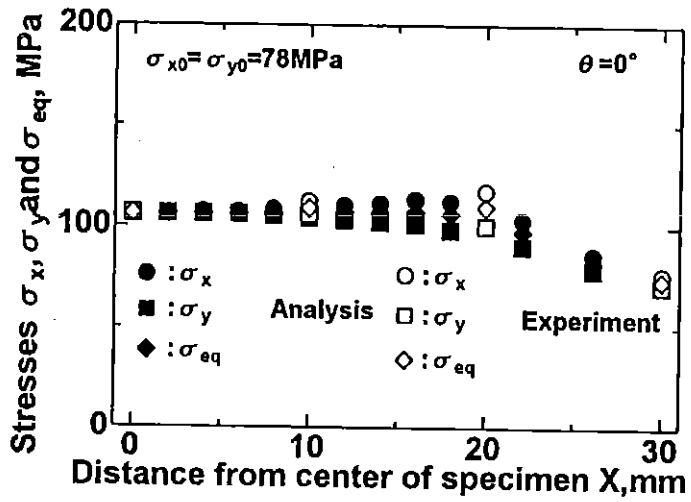

(a) Along X-axis(θ=0°)

Fig. 4 Comparison between stresses calculated and measured in the thickness-reduced region in the Type A cruciform specimen with t=2mm, r_0=18mmand R=74mm under equi-biaxial loadings of $\sigma_{x0}=\sigma_{y0}$=78MPa

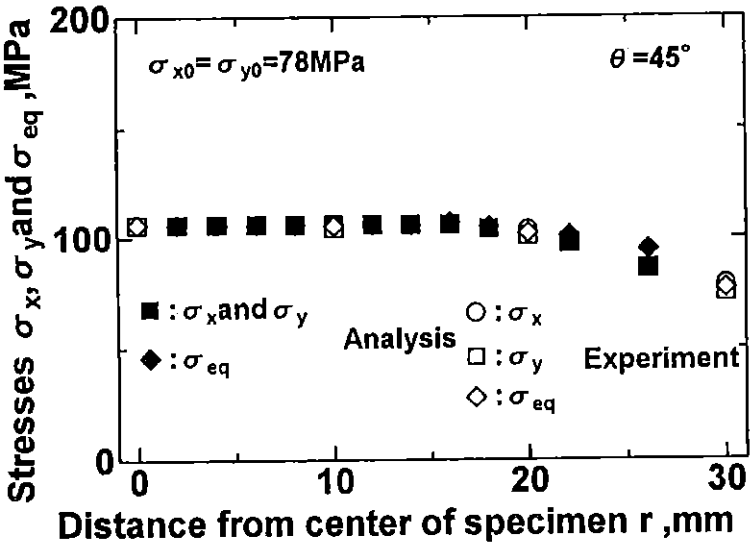

(b)In the direction of θ =45°

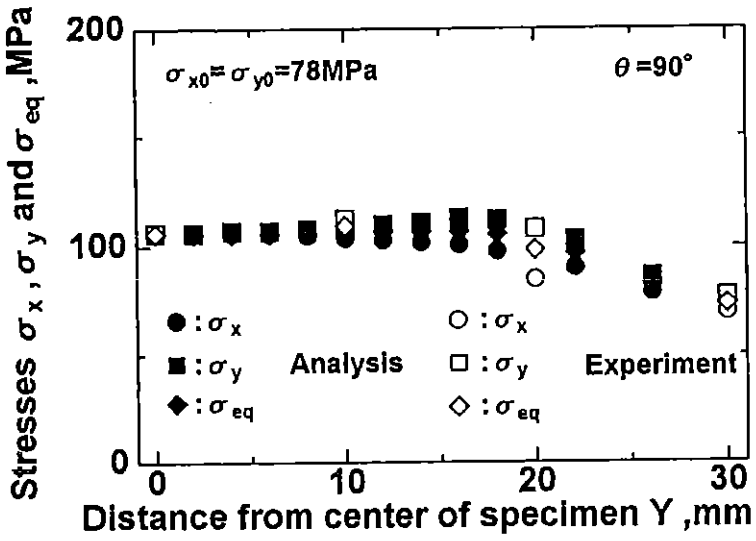

(c) Along Y-axis(θ =90°)

Fig. 4 Comparison between stresses calculated and measured in the thickness-reduced region in the Type A cruciform specimen, with t=2mm, r_0=18mm and R=74mm under equi-biaxial loadings of $\sigma_{x0}=\sigma_{y0}$=78MPa

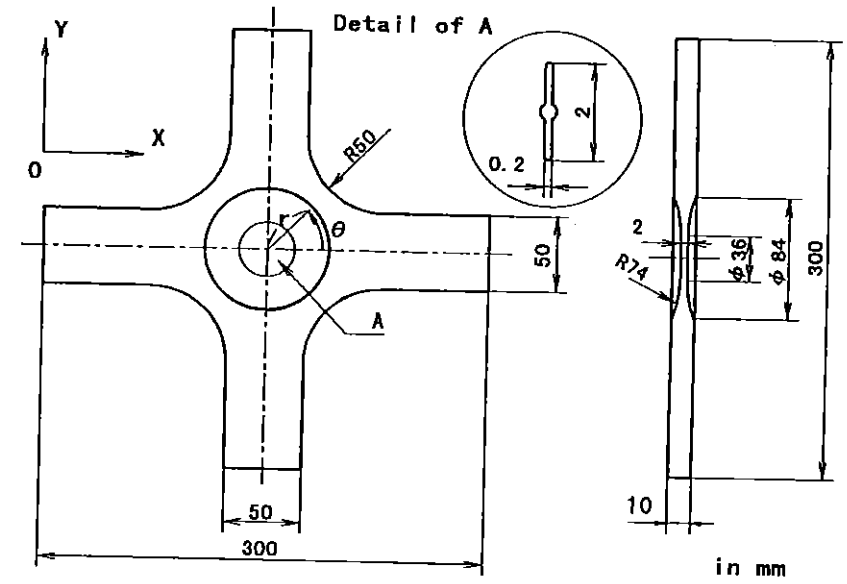

(a) Type A

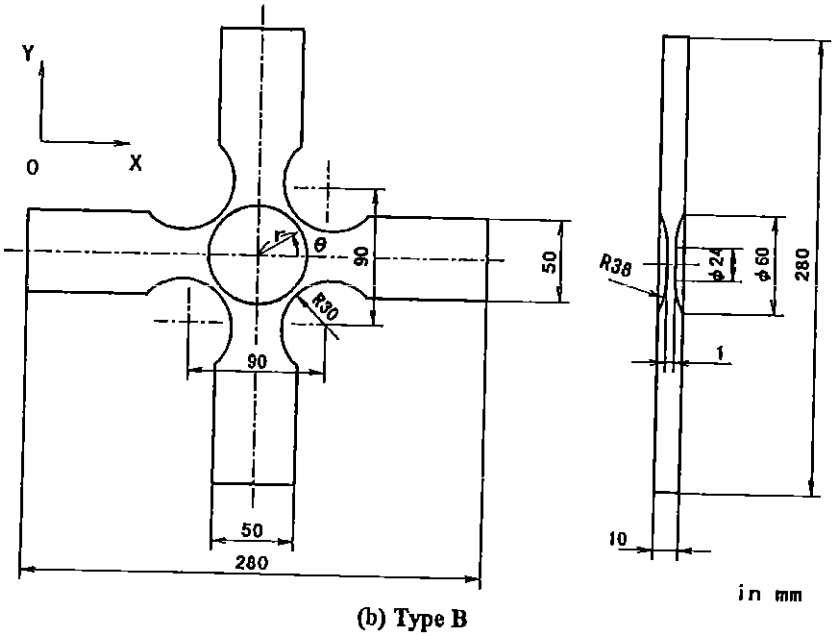

(b) Type B

Fig. 5 Configurations of the designed cruciform specimens

configuration of the specimen determined from such calculations is presented in Fig. 5(a) and this is named the Type A specimen.

The similar calculation procedures are taken for designing an another type of cruciform specimen with the intention of realizing the much higher stress state in the thickness-reduced region than in the Type A specimen. The shape and dimensions of the specimen determined to fulfill this object is shown in Fig. 5(b), which is named the Type B specimen.

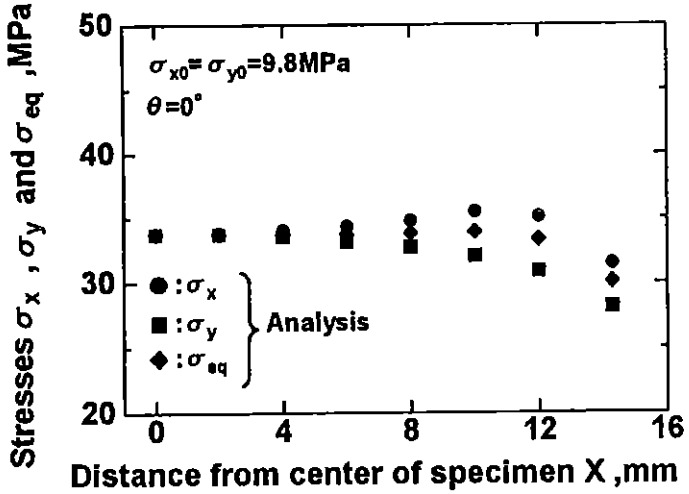

Fig. 6 Distributions of calculated stresses in the thickness-reduced region of the Type B specimen under equi-biaxial loadings of $\sigma_{x0}=\sigma_{y0}$=9.8MPa

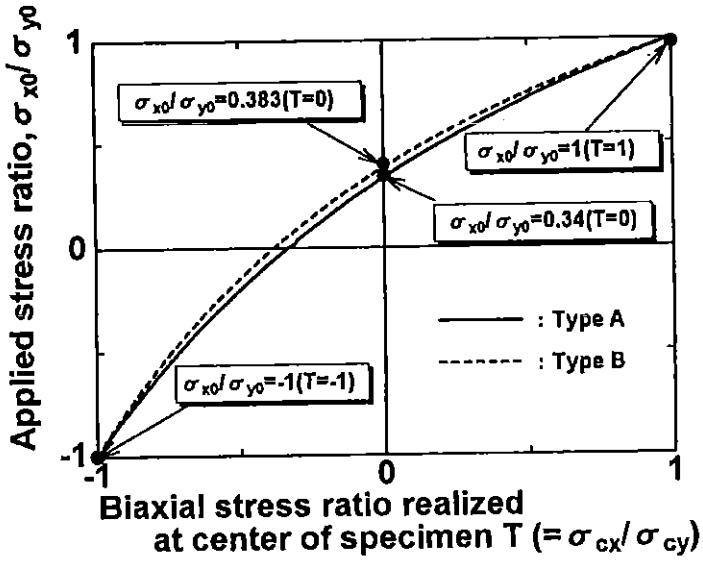

Fig. 7 Calculated relationships between applied stress ratio applied at grip ends and stress ratio realized in the thickness-reduced region

Figure 6 shows the distributions of the three stress components calculated along the X-direction ($\theta = 0^\circ$) in the thickness-reduced region of the Type B specimen under the equi-biaxial stress condition of $\sigma_{x0} = \sigma_{y0} = 9.8$MPa. The differences in the normal stresses in the X- and Y- directions at the position of r=8mm and the center are less than 3.0 percent of the ones at the center. Then the effective test area is determined to be within the circle of r=8mm in the Type B specimen.

The relationships between the ratio of biaxial stresses applied at the grip ends σ_{x0}/σ_{y0} and the biaxial stress ratio realized in the thickness-reduced region $T = \sigma_{ex}/\sigma_{ey}$ were evaluated through the elastic FEM calculation in both the types of the specimens, and were shown in Fig. 7. We can determine from the figure the ratio of the loads to be applied in X- and Y-directions at the grip ends, corresponding to the biaxial stress ratio intended in the thickness-reduced region in both the specimens.

4 Experimental Procedures

Elastic stresses were measured by strain gages and compared with the stresses calculated from the elastic FEM in the thickness-reduced region in the type A specimen. The strain gages were stuck at the locations of r=0, 10, 20 and 30mm in the three directions of $\theta = 0^\circ$, 45° , and 90° . The strain measurements were carried out under uniaxial and equi-biaxial stress conditions which were realized at the biaxial stress ratio $\sigma_{x0}/\sigma_{y0} = 0.34$ and 1.0 at the grip ends, respectively.

The Type A cruciform specimen was fatigue-tested under uniaxial stress condition which is attained by applying the biaxial stresses of the ratio $\sigma_{x0}/\sigma_{y0} = 0.34$ at the grip ends at the stress ratio R=0.1. Then crack growth rate was compared with the test data obtained from a strip type-through-thickness center-cracked specimen. Fatigue crack extension tests were performed at the biaxial stress ratios of T=-1.0, -0.5, 0.5, 0.7, 0.9 and 1.0 besides at the uniaxial stress ratio T=0 for the type B specimen, where a stress ratio and a cyclic frequency were R=-1.0 and f=2.0Hz, respectively.

The strain gages were stuck at the positions of 500 μ m ahead of the pre-crack tip and 1.5mm above the pre-crack ,and cyclic load-strain responses in the Y-direction were measured in the Type B specimen. The abrupt change in the compliance was detected on the measured cyclic load-strain curve and then crack opening point was determined.

5 Estimation of Stress Intensity Factor

The stress intensity factor range ΔK was calculated from the following equation,

$$\Delta K = F(a)\,\Delta\delta\,\sqrt{\pi a}, \qquad (1)$$

where a is half the crack size, $\Delta\sigma$ the stress range in the thickness-reduced region and

F(a) the correction factor of the stress intensity factor, which is determined from the energy method [12] as follows.

The strain energy release rate $\Delta U/\Delta a$ estimated from the change in energy ΔU accompanied by crack extension Δa is related to the stress intensity factor by the equation,

$$K^2/E = \Delta U/(t\,\Delta a), \qquad (2)$$

where E is the Young's modulus and t the thickness of the specimen . In the energy methods ,the quantity $\Delta U/\Delta a$ is assessed by performing stress/strain analysis for the cruciform specimens containing the cracks of 2a and $2(a+\Delta a)$ in size using the elastic FEM: The load-displacement curves were computed for both the X- and Y-directions in the cruciform specimens with the cracks of 2a and $2(a+\Delta a)$ in size. The change in the strain energy ΔU was determined as the difference between the strain energies obtained from the load-displacement responses of the two specimens, which was done for the load-displacement curves in the X- and Y-directions. The sum of the two quantities in the strain energy variation was substituted for ΔU in eq.(2), and then the stress intensity factor was estimated. The correction factor F(a) is calculated from introducing this stress intensity factor into eq.(1). The correction factor F(a) estimated at various biaxial stress ratios in this way is plotted against half the crack size a in Fig. 8, where the F(a) is approximately expressed by the polynomials from which the geometrical correction factor is determined at an arbitrary crack size.

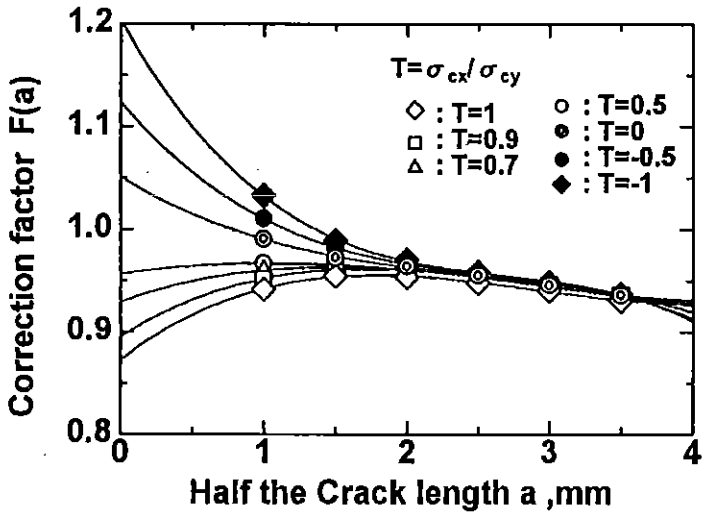

Fig. 8 Correction factor for the stress intensity factor calculated from the energy method as a function of half the crack size

6 Test Results and Discussion

6.1 Comparison of Calculated and Measured Stresses

The normal stresses in the X- and Y-directions and the Mises' type equivalent stress were measured under equi-biaxial stress condition of $\sigma_{x0} = \sigma_{y0} = 78$MPa in the thickness-reduced region by strain gages in the Type A specimen, and are presented in Figs. 4. The figures show the good agreement of the calculated stresses with the experimental data .The same agreement was obtained between the calculated and the measured stresses under the condition loaded separately at the grip ends in the X- and Y-directions. Thus it was confirmed that the stresses calculated under various biaxial stress conditions are uniform and agree well with the measured ones in the thickness-reduced region within the circle of the radius r=10mm.

6.2 Crack Growth Rate

First fatigue crack extension tests were performed under the test condition of biaxial stress ratio T=0 and at stress ratio R=0.1 using both the Type A cruciform specimen and the strip type-through-thickness center-cracked plate specimen, which aimed at verifying

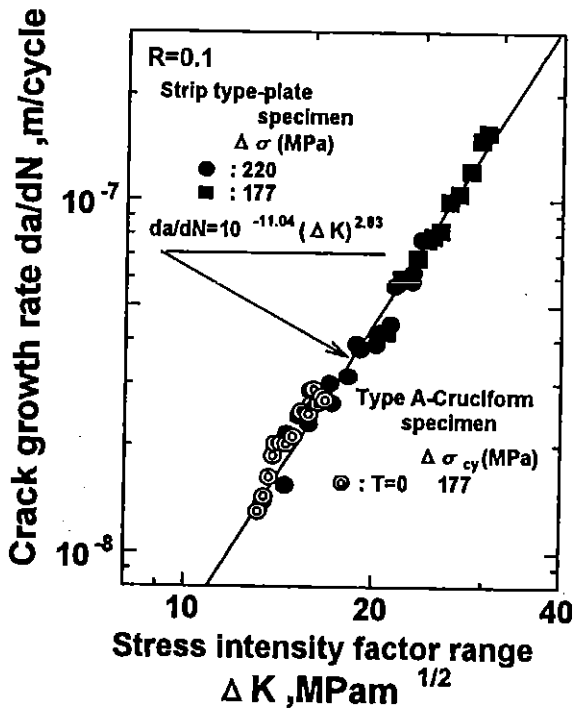

Fig. 9 Relationship between fatigue crack growth rate and stress intensity factor range obtained from the Type A cruciform and center-cracked strip type-plate specimens at R=0.1

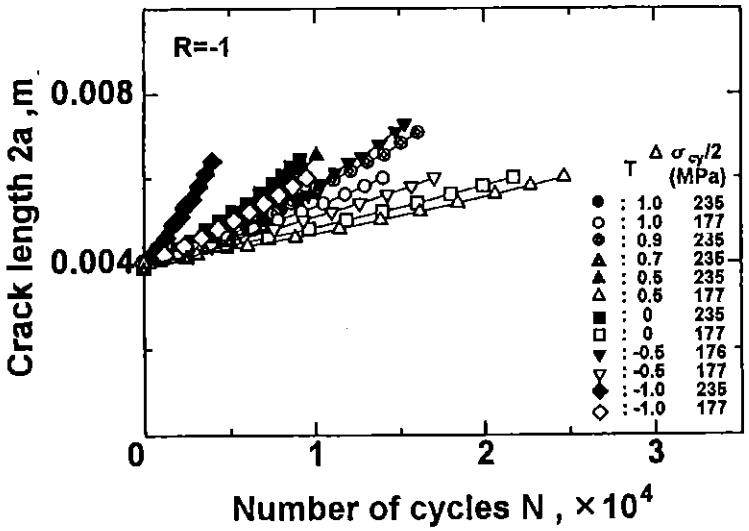

Fig. 10 Fatigue crack growth curves measured in the Type B cruciform specimens at R=-1.0

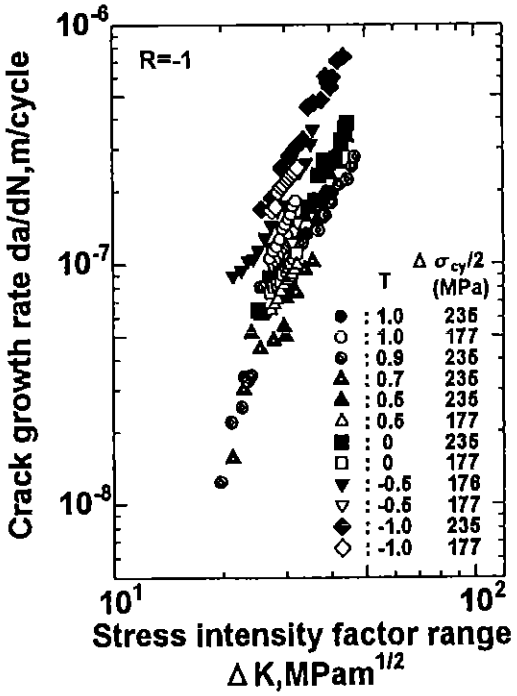

Fig.11 Fatigue crack growth rate plotted against stress intensity factor range, where the Type B specimens were tested at R=-1.0

the appropriateness of the design of the cruciform specimen and the evaluation of the stress intensity factor. The crack growth rate da/dN measured in the tests is plotted against the stress intensity factor range estimated for the cruciform specimen by the energy method in Fig. 9. The relationships between da/dN and ΔK for the cruciform and strip type-plate specimens agree with each other, exhibiting the validity of the test and the evaluation method of the stress intensity factor in the present study.

Figure 10 shows the fatigue crack extension curves obtained from the Type B specimen tested at various biaxial stress ratios at stress ratio $R=-1.0$. The comparison among crack extension curves generally shows that the crack growth rate becomes large with decrease in biaxial stress ratio T except for the case for $T=1.0$ at $\Delta\sigma_{cy}/2=177$MPa, which seems to be unreasonable data due to a scatter in the material property and/or inaccuracy in testing.

The fatigue crack growth rate da/dN estimated from Fig. 10 is plotted against ΔK on double logarithmic scales in Fig. 11. The data denoted by a open circle, which were noted just before are situated on the higher crack growth rate side, compared with the other test data obtained at T larger than zero at $\Delta\sigma_{cy}/2=177$MPa. Except this the relationship between log da/dN and log ΔK tends to move toward the higher crack growth rate as T decrease from 1.0 to -1.0.

7 Crack Opening Load Ratio

Figure 12 shows the crack opening load ratio U plotted against the crack length 2a which

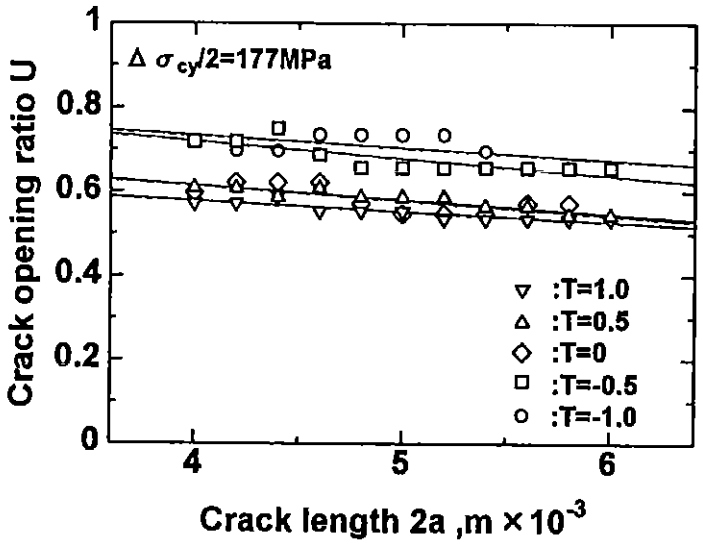

Fig. 12 Relationship between crack opening load ratio and crack size measured in the Type B specimen

was measured at various biaxial stress ratios at $\Delta\sigma_{cy}/2=177$MPa in the Type B specimen. Quite large scatter exists in the U vs. 2a plots. Nevertheless, it is laid down that U has a tendency to decrease with increase in 2a and is greater under test conditions of $T<0$ than $T\geqq 0$. The U-values are plotted for a given crack length as a function of the biaxial stress ratio T in Fig. 13. It is noted that U decreases with increase in T, of which change is large in the range of $T<0$ and quite small in the range of $T\geqq 0$ in its rate.

The effective stress intensity factor range ΔK_{eff} was estimated by multiplying U into ΔK, and the fatigue crack growth rate was plotted against ΔK_{eff} in Fig. 14. The T dependency of the relationship between da/dN and ΔK shown in Fig. 11 disappears in the figure, and the da/dN vs. ΔK_{eff} plots form a unique narrow band independent of T. The crack growth rate data obtained under the test condition of T=1.0 at $\Delta\sigma_{cy}/2=177$MPa, which was marked above, also come to this band. The band is expressed through the least square's regression analysis by the following equation,

$$da/dN=10^{-27.55}(\Delta K_{eff})^{3.94} \qquad (3)$$

8 Calculation of Plastic Strain around the Crack Tip

Elastic-plastic finite element method was applied to the calculation of the plastic strain induced around the crack tip under several biaxial stress conditions. The eight node-isoparametric elements were used for the calculation, where the numbers of the elements and the element-nodes were 260 and 1983, respectively.

Figures 15(a) to (f) show the distributions of the equivalent plastic strain in the vicinity of the crack tip calculated at the biaxial stress ratios T=1.0, 0.5, 0, -0.1 -0.5 and -1.0 under the Y-directed loading of $\sigma_{cy}=177.0$MPa in the Type B specimen, where crack size was 2a=4mm. According to the figures, the tensile loading in the X-direction hardly influences the amount and domain size of the plastic strain around the crack tip: those are almost the same at T=0, 0.5 and 1.0, although the plastic strain region extends slightly in the Y-direction at T=0 compared with the ones at T=1.0 and 0.5. Meanwhile, the compressive stress in the X-direction significantly develops the plastic strain in the vicinity of the crack tip, as shown in (e) and (f); the localized plastic strain extends greatly in the direction of $\theta\cong 45^{\circ}$, being affected by the lateral stress. Specifically, it is noted that quite large amount of plastic strain, $\varepsilon_{peq}=1\times10^{-3}$ is generated just near the crack tip at T=-1.0, as shown in (f). Enhancement of the crack growth rate at the negative biaxial stress ratio, which is shown in Fig. 11, is explained in terms of such a development of the localized plastic strain around the crack tip. The crack opening and closure are sensitively influenced by the plastic strain occurring in the vicinity of the fatigue crack tip. The biaxial stress ratio dependent crack opening load ratio presented in Fig. 13 is also interpreted from the T-dependent localized plastic strain behaviors around the crack tip shown in Figs. 15. The T dependency of the fatigue crack growth rate disappears against the effective stress intensity factor range which includes such a localized plastic strain effect, as shown in Fig. 14.

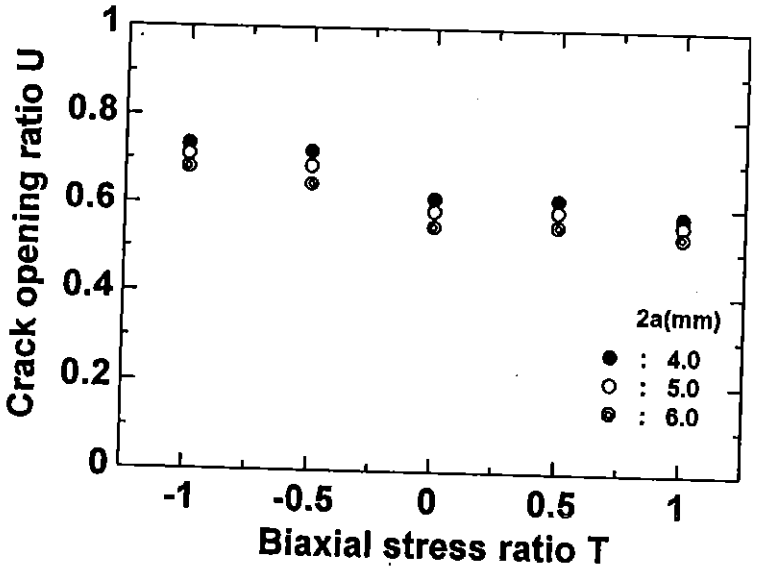

Fig. 13 Crack openig load ratio plotted against biaxial stress ratio, which was measured at a given crack size in the type B specimen

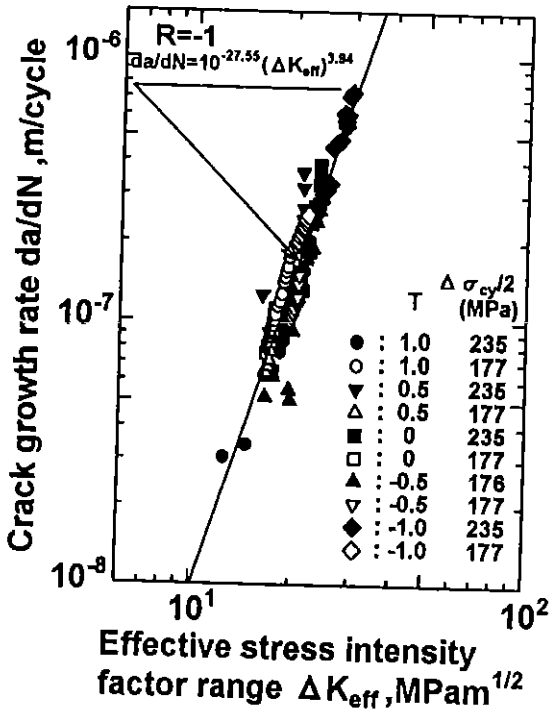

Fig. 14 Relationship between fatigue crack growth rate plotted against effective stress intensity factor range in the Type B specimen

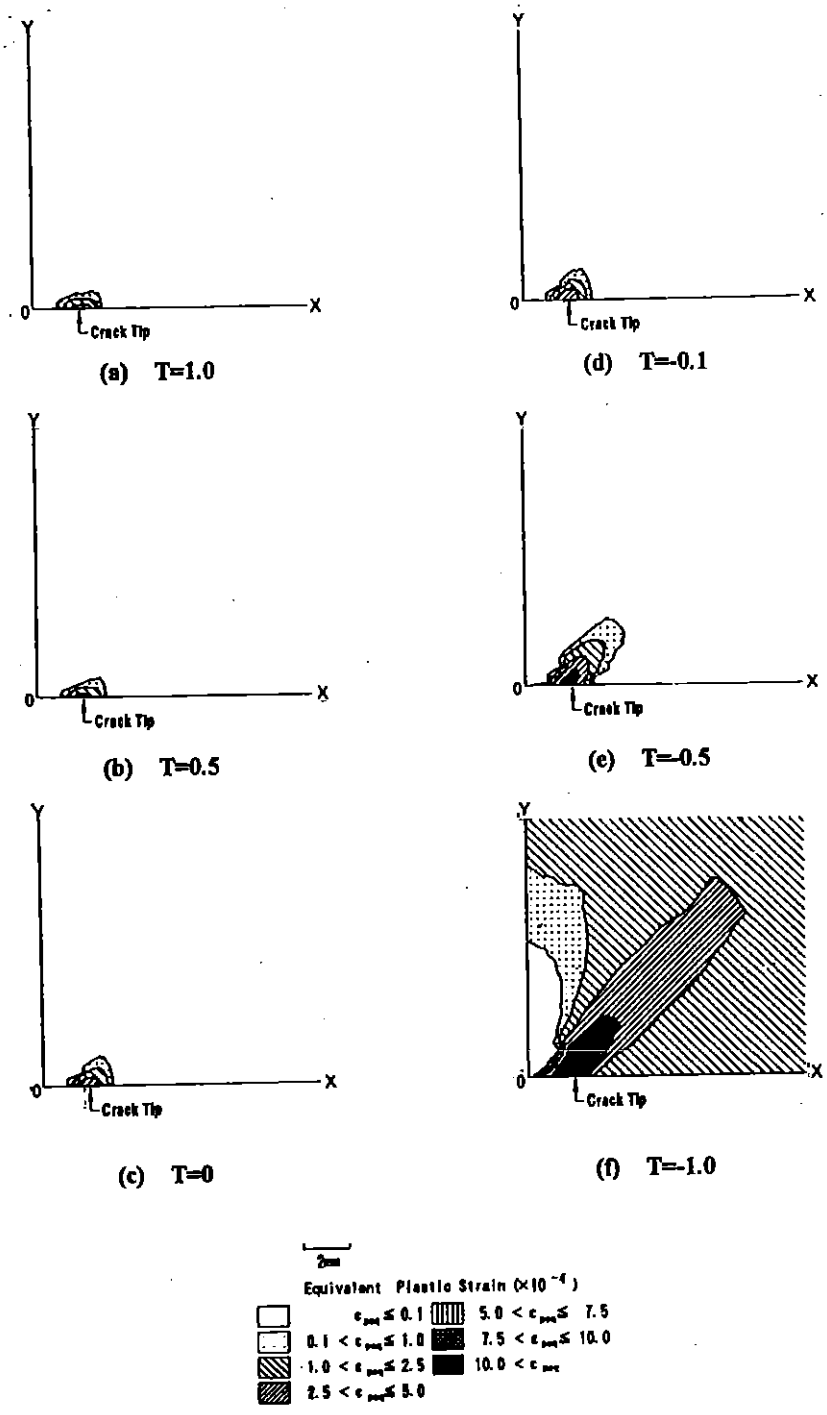

Fig.15 Equivalent plastic strain calculated in the vicinity of crack tip at σ_{cy}=177MPa, where crack size is 2a=4.0mm

9 Conclusions

The cruciform specimen was newly designed for examinig the fatigue behaviors under widely ranged biaxial loadings through the stress/strain analysis using the elastic finite element method. The fatigue crack extension tests were performed for the cruciform specimen machined from JIS S45C steel at biaxial stress ratios T=-1.0, -0.5, 0, 0.5 0.7 0.9 and 1.0 at stress ratios R=-1.0 and 0.1. The crack closure was measured during the test and the crack growth rate was analyzed in terms of fracture mechanics parameters. Furthermore, the plastic strain was estimated in the vicinity of crack tip under several biaxial static loading ratios using the elastic-plastic FEM. Main results obtained are summarized as follows.

(1) The stress raising and the uniformity in the raised stress were realized within the circles of radii r=10 and 8mm in the thickness-reduced region in the designed cruciform specimens of Types A and B.

(2) The fatigue crack growth rate da/dN is accelerated under cyclic loadings of the negative biaxial stress ratios T=-1.0 and -0.5, while cyclic loadings of the positive biaxial stress ratios T=0.5 and 1.0 tend to decrease crack growth rate to some extent.

(3) Crack opening load ratio decreases as crack extends and is much more enhanced under loading conditions of T<0 than T>0.

(4) The fatigue crack growth rate plotted against the stress intensity factor range ΔK exhibits the biaxial stress ratio dependency: the da/dN vs. ΔK plots is situated on the higher crack growth rate side under the loading conditions of T<0 than T>0.

(5) The calculation shows that the plastic strain develops around the crack tip much more under the loading conditions of T<0 than T>0. This corresponds well to the higher crack growth rate and the greater crack opening load ratio under the former than under the latter.

(6) The biaxial stress ratio dependency of the crack growth rate disappears in the relationship between da/dN and the effective stress intensity factor range ΔK_{eff}, which forms a common narrow band characteristic of S45C steel.

Acknowledgement

The financial support to this work by the New Energy and Industrial Technology Revelopment Organization in Japan is gratefully acknowledged.

References

(1)Sakane, M., Ohnami, M., Kuno, T. and Izumura, T., 1987, High Temperature Biaxial Low Cycle Fatigue Using Cruciform Specimen, J. Soc. Mat. Sci. Japan., 37, 340-346, (in Japanese).

(2)Sakane, M., Itoh, T.and Ohnami, M., 1990, Crack Mode in High-Temperature Biaxial Low Cycle Fatigue Using a Cruciform Specimen, Trans. Jpn. Soc. Mech. Eng., 56, 1549-

1556,(in Japanese).
(3)Lam, Y. C., Fatigue Crack Growth under Biaxial Loading, 1993, Fatigue Fract. Eng. Mater. Struct., **16**, 429-440.
(4)Hoshide, T., Tanaka, K. and Yamada, A., 1981, Stress-Ratio Effect of Fatigue Crack Propagation in a Biaxial Stress Field, Fatigue Eng. Mater. Struct., **4**, 355-366.
(5)Yuuki, R., Kitagawa, H., Tohgou, K.and Tanabe, M., 1981, The Efect of Biaxial Stresses on Fatigue Crack Growth and the Factors Influencing it, Trans. Jpn. Soc. Mech. Eng., **51**, 2057-2066, (in Japanese).
(6)Miller, K. J., 1977, Fatigue under Complex Stress, Metals Sci., **11**, 432-438.
(7)Miller, K. J. and Brown, M. W., 1985, Mode I Fatigue Crack Growth under Biaxial Stress at Room and Elevated Temperatures, ASTM STP, **853**, 135-152.
(8)Tanaka, K., Hoshide, T., Yamada, A. and Taira, S., 1979, Fatigue Crack Propagation in Biaxial Stress Fields, Fatigue Eng. Mater. Struct., **2**, 181-194.
(9)Kitagawa, H., Yuuki, R., Tohgou, K. and Kakuta, Y., 1979, Fracture Mechanical Approach to Fatigue Crack Growth in High Strength Steel Plate under In-Plane Biaxial Loads, Trans. Jpn. Soc. Mech. Eng., **45**, 707-716, (in Japanese)..
(10) Yuuki, R., Kitagawa, H. and Tohgou, K., 1981, The Threshold Condition and Closure Behavior of Fatigue Crack under Biaxial Loads, Trans. Jpn. Soc. Mech. Eng., **47**, 981-989, (in Japanese)..
(11)Liu, A. F., Allison, J. E., Dittmer, D. F. and Yamane, J. R., 1979, Effect of Biaxial Stresses on Crack Growth, ASTM STP, **677**, 5-22.
(12)Ishida, M., 1976, Elastic Stress/Strain Analysis and Stress Intensity Factor, Monograph Series, No.2, Fracture Mechanics and Strength of Materials, Baihukan, P. 58, (in Japanese).